

# TANDEM: Temporal Attention-guided Neural Differential Equations for Missingness in Time Series Classification

YongKyung Oh

yongkyungoh@mednet.ucla.edu  
University of California, Los Angeles,  
Los Angeles, CA, USA

Sungil Kim\*

sungil.kim@unist.ac.kr  
Ulsan National Institute of Science and Technology,  
Ulsan, Republic of Korea

Dong-Young Lim

dlim@unist.ac.kr  
Ulsan National Institute of Science and Technology,  
Ulsan, Republic of Korea

Alex A. T. Bui\*

buia@mii.ucla.edu  
University of California, Los Angeles,  
Los Angeles, CA, USA

## Abstract

Handling missing data in time series classification remains a significant challenge in various domains. Traditional methods often rely on imputation, which may introduce bias or fail to capture the underlying temporal dynamics. In this paper, we propose TANDEM (*Temporal Attention-guided Neural Differential Equations for Missingness*), an attention-guided neural differential equation framework that effectively classifies time series data with missing values. Our approach integrates raw observation, interpolated control path, and continuous latent dynamics through a novel attention mechanism, allowing the model to focus on the most informative aspects of the data. We evaluate TANDEM on 30 benchmark datasets and a real-world medical dataset, demonstrating its superiority over existing state-of-the-art methods. Our framework not only improves classification accuracy but also provides insights into the handling of missing data, making it a valuable tool in practice.

## CCS Concepts

• Computing methodologies → Artificial intelligence; Machine learning.

## Keywords

Time series classification, Missing data, Neural differential equations, Attention mechanism, Temporal dynamics

## ACM Reference Format:

YongKyung Oh, Dong-Young Lim, Sungil Kim[1], and Alex A. T. Bui. 2025. TANDEM: Temporal Attention-guided Neural Differential Equations for Missingness in Time Series Classification. In *Proceedings of the 34th ACM International Conference on Information and Knowledge Management (CIKM '25), November 10–14, 2025, Seoul, Republic of Korea*. ACM, New York, NY, USA, 11 pages. <https://doi.org/10.1145/3746252.3760996>

\*Corresponding authors

Permission to make digital or hard copies of all or part of this work for personal or classroom use is granted without fee provided that copies are not made or distributed for profit or commercial advantage and that copies bear this notice and the full citation on the first page. Copyrights for components of this work owned by others than the author(s) must be honored. Abstracting with credit is permitted. To copy otherwise, or republish, to post on servers or to redistribute to lists, requires prior specific permission and/or a fee. Request permissions from [permissions@acm.org](mailto:permissions@acm.org).

CIKM '25, Seoul, Republic of Korea.

© 2025 Copyright held by the owner/author(s). Publication rights licensed to ACM. ACM ISBN 979-8-4007-2040-6/2025/11  
<https://doi.org/10.1145/3746252.3760996>

## 1 Introduction

Time series data are fundamental in many domains but are often suffer from missing values due to sensor issues, data corruption, or irregular sampling [31, 43]. Traditional methods for handling missingness, such as deletion or simple imputation, can distort temporal dynamics and introduce bias, especially with non-random or extensive missing data [13, 18]. While generative imputation models [5, 52] offer improvements, they often treat imputation as a separate preprocessing step, potentially neglecting uncertainties and complex dependencies in irregularly sampled time series.

Neural Differential Equations (NDEs), including Neural ODEs [7], CDEs [23], and SDEs [38, 49], provide a robust framework for modeling continuous-time dynamics, adept at handling complex and irregularly sampled data. Neural CDEs, for example, effectively model irregular series by using an input-derived control path to drive the hidden state dynamics. However, NDEs alone do not explicitly address how to best utilize available information when observations are sparse or incomplete for classification tasks [37]. Attention mechanisms [50], renowned for enabling models to focus on salient input segments, offer a promising way to enhance NDEs in such scenarios by adaptively weighing data importance [47, 51].

While the integration of NDEs and attention is an active research area [8, 16, 19, 22, 48], a comprehensive framework that adaptively fuses diverse NDE-derived representations under varying missingness conditions, across multiple NDE backbones, remains less explored. To address this, we propose TANDEM (*Temporal Attention-guided Neural Differential Equations for Missingness*). TANDEM synergistically combines NDEs with a novel attention and gating mechanism to classify time series with missing values. It integrates three feature streams: raw observations, control path, and continuous NDE-derived latent dynamics. A Gumbel-Sigmoid gating module with multi-head attention fuses these streams and prioritizes informative signals under missingness. Our contributions are:

- Novel framework, TANDEM, that integrates raw, interpolated, and latent NDE-based representations to handle missingness in time series. Flexible Gumbel-Sigmoid gating mechanism with multi-head attention for adaptive fusion of these feature streams, enhancing robustness under high missingness.
- A modular design supporting various NDE backbones (Neural ODEs, CDEs, SDEs), allowing users to tailor the continuous-time model to their data.

- Extensive validation on 30 UCR/UEA benchmarks and a real-world medical dataset, demonstrating superior classification accuracy and robustness over state-of-the-art methods across diverse missingness levels.

This paper is organized as follows: Section 2 reviews related work. Section 3 details the TANDEM framework. Experimental results are presented in Section 4 (benchmarks) and Section 5 (real-world application). Section 6 concludes and discusses future work.

## 2 Related Works

NDEs have emerged as a powerful paradigm for modeling continuous-time dynamics [37]. The foundational Neural ODEs [7] parameterize the derivative of a system’s hidden state with a neural network, offering flexibility for irregularly sampled data. Enhancements include Augmented Neural ODEs [12] for increased expressiveness, and Latent ODEs [42] which learn dynamics in a latent space, beneficial for series with missingness. Neural CDEs [23] generalize Neural ODEs by incorporating an input-derived control path, making them highly effective for irregular time series. This was further extended by Neural Rough Differential Equations (Neural RDEs) using rough path theory to handle noisy, long sequences [36]. Concurrently, Neural SDEs have been developed to capture stochastic dynamics. Tzen and Raginsky [49] introduced Neural SDEs for learning stochastic processes, Li et al. [27] addressed scalable gradient computation for them, and Oh et al. [38] analyzed their stability for irregular data. While these NDE methods excel at modeling continuous dynamics, they often lack explicit mechanisms to adaptively prioritize information from different feature representations when faced with missing observations, a gap our work addresses.

*Attention Mechanisms in Sequence Modeling.* Attention mechanisms, first prominent in neural machine translation [2], enable models to dynamically focus on relevant parts of an input sequence. The transformer architecture [50], centered around self-attention, further established this approach for capturing dependencies in sequences. In time series analysis, attention has been used to capture temporal patterns and feature importance. For instance, Qin et al. [39] proposed dual-stage attention for prediction, Shih et al. [46] introduced temporal pattern attention for multivariate forecasting, and Lim et al. [29] developed temporal fusion transformers for interpretable multi-horizon forecasting. These methods highlight the utility of attention in focusing on critical time steps or features.

*Integrating NDEs and Attention Mechanisms.* The integration of NDEs with attention mechanisms, which combines continuous-time modeling with dynamic input weighting, is an active research area. Initial explorations often occurred in Natural Language Processing (NLP). ODE Transformer [26] models attention dynamics as a discretized ODE process for sequence generation tasks. Zhang et al. [53] introduced a continuous self-attention mechanism via Neural ODEs, evolving representations over continuous depth. More recently, Tong et al. [48] further analyzed the internal dynamics of Neural ODE Transformers and proposed adaptive fine-tuning.

In the time series domain, efforts to combine these paradigms include ACE-NODE (Attentive Co-Evolving Neural Ordinary Differential Equations) by Jhin et al. [19], which integrates attention with Neural ODEs, and research by J.-T. Chien and Y.-H. Chen [16]

on continuous-time self-attention within NDEs. ANCDE (Attentive Neural Controlled Differential Equation) [22] applied attention mechanisms specifically to the control paths in Neural CDEs.

While these represent valuable advancements, they often target specific NDE backbones or particular attention integration strategies. A comprehensive framework that supports multiple NDE types (Neural ODE, CDE, SDE), adaptively fuses diverse feature representations via explicit gating, and is tailored for robust classification under various missing data conditions, remains a key area for development. TANDEM is designed to address this gap by providing a unified, attention-guided mechanism to dynamically weigh and combine these distinct information sources.

*Differentiable Gating for Feature Selection.* Relying on a single stream can obscure missingness patterns or limit expressivity [30]. Prior works such as [47, 51] use attention to learn from raw input features directly, but often lack mechanisms to selectively weight fundamentally different representation types. On the other hand, interpolated paths provide global trends [23], and NDEs capture latent dynamics [42]. Although these features are complementary, there remains a gap in effectively integrating them. Effectively selecting relevant information streams is a core challenge in multi-source integration. The Gumbel-Softmax trick [17, 33] addresses this by enabling differentiable, near-discrete selection through continuous relaxation of categorical variables, allowing end-to-end training of selection mechanisms within model. Based on that, TANDEM tackles this challenge by integrating raw, interpolated, and latent features using Gumbel-based differentiable gating, enabling adaptive and near-discrete fusion guided by multi-view learning principles.

## 3 Methodology

The TANDEM framework is designed to perform robust time series classification. It achieves this by adaptively integrating multiple feature representations derived from the input series and its continuous latent dynamics, as conceptually illustrated in Figure 1.

*Problem Formulation.* We consider an  $\mathbb{R}^d$ -valued time series as  $\mathbf{x} = (x(1), \dots, x(T))$ , where each observation  $x(t)$  is a  $d$ -dimensional vector. In many practical settings, observations can be missing or incomplete. We represent this missingness using a binary mask  $M = (M(1), \dots, M(T))$ , where  $M(t) \in \{0, 1\}^d$ . An entry  $M(t)_j = 0$  signifies that the  $j$ -th dimension of  $x(t)$  is missing, while  $M(t)_j = 1$  indicates it is observed. The resulting time series with potentially missing values is denoted as  $\tilde{\mathbf{x}} = (\tilde{x}(1), \dots, \tilde{x}(T))$ , where  $\tilde{x}(t) = M(t) \odot x(t)$ , with  $\odot$  representing the element-wise product. Given a dataset  $\mathcal{D} = \{(\tilde{\mathbf{x}}^{(i)}, M^{(i)}, y^{(i)})\}_{i=1}^N$  consisting of  $N$  such time series, where  $y^{(i)} \in \{1, \dots, C\}$  is the class label for the  $i$ -th series, our objective is to learn a classifier  $f : \mathbb{R}^{d \times T} \times \{0, 1\}^{d \times T} \rightarrow \{1, \dots, C\}$  that accurately predicts  $y$  for a given  $\tilde{\mathbf{x}}$  and  $M$ .

### 3.1 Multi-Perspective Feature Extraction

To effectively handle missing data and capture the underlying temporal dynamics, TANDEM utilizes three distinct yet complementary feature representations extracted from the input time series. As illustrated in Figure 1, these features offer different perspectives on the data: (i) the raw, potentially incomplete, observations; (ii) an interpolated continuous control path; and (iii) continuous latent

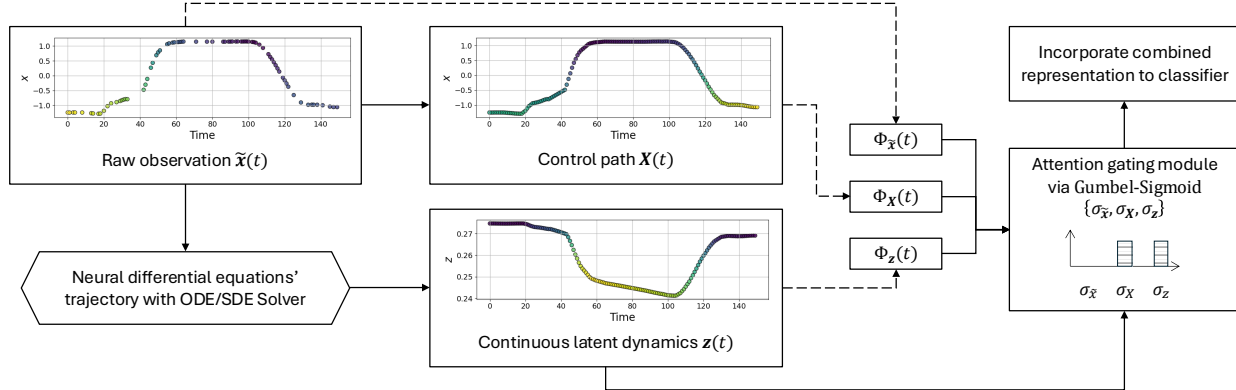


**Figure 1: Conceptual overview of the TANDEM framework.** For a given time series with potentially missing values, three distinct feature streams are processed: (i) the raw observation  $\tilde{x}(t)$ , (ii) an interpolated, piecewise-smooth control path  $X(t)$ , and (iii) continuous latent dynamics  $z(t)$  derived from an NDE backbone. Each stream is individually refined by attention mechanisms, resulting in attended representations  $\Phi_{\tilde{x}}(t)$ ,  $\Phi_X(t)$ , and  $\Phi_z(t)$ . Colors represent the learned temporal attention scores for each stream. These attended representations are then adaptively weighted by learnable Gumbel-Sigmoid gates  $(\sigma_{\tilde{x}}, \sigma_X, \sigma_z)$  which determine the contribution of each stream. The resulting fused representation,  $\bar{z}(t)$ , is subsequently passed to a classifier.

dynamics modeled by a NDE. These representations are complementary to one another and are subsequently fused.

**Raw Observation ( $\tilde{x}(t)$ ).** The primary input is the raw observed time series  $\tilde{x}(t) \in \mathbb{R}^d$ . This stream provides the model with the actual observed data points at discrete time steps, including any missing entries. Preserving raw observations is crucial because the pattern of missingness itself can sometimes be informative [30], and the observed values, however sparse, constitute the most direct evidence of the system’s state.

**Interpolated Control Path ( $X(t)$ ).** To derive a continuous representation from potentially irregular and incomplete raw observations, we construct an interpolated control path,  $X(t)$ . This path offers a smooth, continuous trajectory that spans missing segments and effectively regularizes the input signal. This approach is chosen for its ability to produce a smooth curve that passes through all observed data points, providing a continuously differentiable path that is beneficial for certain NDEs, such as Neural CDEs [23]. Given the set of observed points  $\{(t_k, \tilde{x}(t_k))\}$  where  $M(t_k)_j = 1$  for relevant dimensions, the spline  $X(s)$  for  $s \in [0, T]$  yields this continuous function. The control path  $X(t)$  acts as an initial continuous approximation that guides the NDE backbone and provides a complete representation of the time series trajectory for subsequent attention-based processing.

**Continuous Latent Dynamics ( $z(t)$ ).** To model the underlying generative process and learn a representation of the system’s dynamics in a continuous latent space, we utilize NDEs as backbone models. The hidden trajectory  $z(t) \in \mathbb{R}^{d_z}$  aims to capture the evolving state of the system. Based on the assumed nature of these dynamics, different NDE backbones can be employed within our framework:

- **Neural ODEs** [7] describe deterministic dynamics:

$$z(t) = z(0) + \int_0^t f(s, z(s); \theta_f) ds. \quad (1)$$

Here,  $f$  is a neural network parameterizing the derivative, and the initial state  $z(0)$  is typically learned via another neural network  $\eta(x_{\text{init}}; \theta_\eta)$  based on an initial segment or summary of  $\tilde{x}$ .

- **Neural CDEs** [23] model dynamics as controlled by the input path  $X(t)$ :

$$z(t) = z(0) + \int_0^t f(s, z(s); \theta_f) dX(s). \quad (2)$$

The Riemann-Stieltjes integral allows  $z(t)$  to respond dynamically to the continuous signal  $X(t)$ .

- **Neural SDEs** [38, 49] introduce stochasticity:

$$z(t) = z(0) + \int_0^t f(s, z(s); \theta_f) ds + \int_0^t g(s, z(s); \theta_g) dB(s), \quad (3)$$

where  $f$  is the drift function,  $g$  is the diffusion function, and  $B(t)$  represents a Brownian motion.

These NDEs yield a continuous representation  $z(t)$  that naturally accommodates irregular sampling. This representation provides a dynamically evolving summary of the time series, capable of inferring behavior even across missing segments. The flexibility to choose among different NDEs allows for tailoring the model to various types of temporal dependencies. The vector fields  $f$  (and  $g$ ) are parameterized by neural networks.

### 3.2 Adaptive Feature Fusion with Gating

To effectively leverage the complementary information from the three extracted feature streams, we introduce an adaptive fusion mechanism. This mechanism comprises two key components: (1) a feature-wise multi-head attention module to capture the relevance of different dimensions within each feature stream at each time step, and (2) a stream-wise gating module employing a Gumbel-Sigmoid distribution to dynamically select or weigh the contribution of each entire feature stream.

**3.2.1 Feature-wise Multi-head Attention.** We first apply a multi-head attention mechanism [50] independently to each of the three

feature streams:  $\tilde{x}(t) \in \mathbb{R}^d$ ,  $X(t) \in \mathbb{R}^d$ , and  $z(t) \in \mathbb{R}^{d_z}$ . This step allows the model to weigh the importance of different dimensions or learned features within each individual stream at every time point  $t$ . For a generic feature stream  $\phi_k(t)$  (where  $k$  indexes one of the three streams: raw, control, or latent), we project it into query ( $Q_k^h(t)$ ), key ( $K_k^h(t)$ ), and value ( $V_k^h(t)$ ) representations for each attention head  $h \in \{1, \dots, H\}$ :

$$Q_k^h(t) = W_{Q,k}^h \phi_k(t), \quad K_k^h(t) = W_{K,k}^h \phi_k(t), \quad V_k^h(t) = W_{V,k}^h \phi_k(t), \quad (4)$$

where  $W_{Q,k}^h$ ,  $W_{K,k}^h$ ,  $W_{V,k}^h$  are trainable weight matrices specific to feature stream  $k$  and head  $h$ . The attention weights for each head are computed using scaled dot-product attention:

$$\text{attn\_weights}_k^h(t) = \text{softmax} \left( \frac{Q_k^h(t)^T K_k^h(t)}{\sqrt{d_{key}}} \right), \quad (5)$$

where  $d_{key}$  is the dimension of the key vectors. The attended feature representation for stream  $k$  from head  $h$  is then  $\Phi_k^h(t) = \text{attn\_weights}_k^h(t) V_k^h(t)$ . The outputs from all heads are subsequently concatenated and linearly projected to produce the final attended representation for each stream:

$$\Phi_k(t) = W_{O,k} [\Phi_k^1(t); \dots; \Phi_k^H(t)], \quad (6)$$

where  $W_{O,k}$  is a trainable output weight matrix for stream  $k$ . This process yields the attended representations  $\Phi_{\tilde{x}}(t)$ ,  $\Phi_X(t)$ , and  $\Phi_z(t)$ . In Figure 1, the learned attention scores are visualized using different colors. For the latent dynamics  $z$ , we plot the average value of the hidden states for clarity.

An element-wise sigmoid function is applied to each  $\Phi_k(t)$ . The primary role of this sigmoid activation is to normalize the output of the attention module for each stream. It aims to ensure that no single attended stream disproportionately influences the fusion due to its scale, rather than its learned importance, before the explicit gating mechanism determines its contribution.

**3.2.2 Stream-wise Gating via Gumbel-Sigmoid.** While feature-wise attention refines each stream internally, a mechanism is also needed to determine the overall importance or reliability of each entire attended stream ( $\Phi_{\tilde{x}}(t)$ ,  $\Phi_X(t)$ ,  $\Phi_z(t)$ ), particularly under varying conditions of data missingness. For this purpose, we introduce a stream-wise gating mechanism employing a Gumbel-Sigmoid distribution. We opt for the Gumbel-Sigmoid [17, 33] over a standard softmax across streams because it allows the model to select any subset of features independently. This contrasts with softmax, which forces a fixed probability mass (summing to 1) to be distributed across the streams.

We introduce learnable logits,  $\ell_{\tilde{x}}$ ,  $\ell_X$ , and  $\ell_z$ , which correspond to the desirability or relevance of each attended feature stream. The gating value  $\sigma_k$  for each stream  $k \in \{\tilde{x}, X, z\}$  is then computed using the Gumbel-Sigmoid function:

$$\sigma_k = \text{Sigmoid} \left( \frac{\ell_k + \mathcal{G}_k}{\tau} \right), \quad (7)$$

where  $\mathcal{G}_k = -\log(-\log(U_k))$  with  $U_k \sim \text{Uniform}(0, 1)$  are independent Gumbel noise samples. The temperature parameter  $\tau > 0$

controls the smoothness of this approximation: as  $\tau \rightarrow 0$ ,  $\sigma_k$  approaches a Bernoulli variable, thereby emulating a hard selection. During the training phase, we utilize a fixed temperature  $\tau = 1.0$  to ensure differentiability and enable gradient propagation. For inference, one can either use these soft gate values directly or apply hard thresholding for an explicit selection:

$$\sigma_k^{\text{hard}} = \mathbb{I}(\sigma_k > 0.5), \quad (8)$$

where  $\mathbb{I}(\cdot)$  denotes the indicator function. In this study, we use the soft gates  $\sigma_k$  derived from Eq. (7) during both training and inference, unless specified otherwise in ablation studies (e.g., distinguishing ‘TANDEM (soft)’ versus ‘TANDEM’).

The NDE’s latent state  $z(t)$  provides a foundational continuous-time dynamic representation. The information from the gated, attended feature streams is then combined to form the final representation for classification. The final combined feature representation  $\tilde{Z}(t)$ , which is passed to the classifier, is formed by a weighted aggregation of these attended and gated features:

$$\tilde{Z}(t) = \sigma_{\tilde{x}} \Phi_{\tilde{x}}(t) \oplus \sigma_X \Phi_X(t) \oplus \sigma_z \Phi_z(t) \quad (9)$$

where  $\oplus$  indicates a concatenation, depending on the input requirements of  $f_{\text{classifier}}$ . The key aspect is that the gates  $\sigma_k$  modulate the influence of each fully attended feature stream  $\Phi_k(t)$ .

### 3.3 Optimization for Classification

The final fused feature representation  $\tilde{Z}(t)$ , as defined in Eq. (9), provides a comprehensive summary of the time series, conditioned on the observed data and learned dynamics. For classification, we typically use the representation at the final time point,  $\tilde{Z}(T)$ , or alternatively, a pooled representation across all time steps, as input to a classification head. This head is tasked with mapping the learned temporal representation to a probability distribution over the  $C$  possible class labels.

In this work, we employ a standard feed-forward neural network as the classifier: specifically, a two-layer Multilayer Perceptron (MLP). This MLP utilizes a ReLU activation function in its hidden layer, followed by a Softmax activation function in the output layer to produce the final class probabilities. The dimensionality of the hidden layer is typically set to be consistent with the dimension of the input representation  $\tilde{Z}(T)$ . Denoting the classifier as  $f_{\text{classifier}}(\cdot; \theta_{\text{classifier}})$ , where  $\theta_{\text{classifier}}$  represents its trainable parameters, the predicted class probabilities  $\hat{y}$  are obtained as:

$$\hat{y} = f_{\text{classifier}}(\tilde{Z}(T); \theta_{\text{classifier}}). \quad (10)$$

A crucial aspect of our TANDEM framework is that all its components are trained end-to-end. The optimization is driven by minimizing the standard cross-entropy loss function, suitable for multi-class classification tasks:

$$\mathcal{L}(\Theta) = -\frac{1}{N} \sum_{i=1}^N \sum_{c=1}^C y_c^{(i)} \log \hat{y}_c^{(i)}, \quad (11)$$

where  $\Theta$  encompasses all trainable parameters of the model,  $N$  is the number of time series instances in the training set, and  $y_c^{(i)}$  is the one-hot encoded true label for the  $i$ -th time series for class  $c$ . We employ gradient-based optimization algorithms, such as Adam [24], to minimize this loss function. Specific details regarding the hyperparameter settings, including learning rates and the use of

potentially different learning rates for the final classifier layer to facilitate fine-tuning, are provided in Section 4 and the Appendix. This end-to-end training paradigm ensures that all parts of the model, from feature extraction and NDE modeling to attention-based fusion and gating, are optimized jointly to maximize classification performance on the target task, effectively learning to navigate the challenges posed by missing data.

## 4 Experiment on benchmark datasets

All experiments were performed using a server on Ubuntu 22.04 LTS, equipped with an Intel(R) Xeon(R) Gold 6242 CPU and a cluster of NVIDIA A100 40GB GPUs. The source code for our experiments can be accessed at <https://github.com/yongkyung-oh/TANDEM>.

**Table 1: Data description for the time series datasets used in our experiments: dataset name, number of samples, number of classes, number of dimensions (variables) in each time series, and the length (time steps) of each time series.**

Dataset	# samples	# classes	# dimension	# length
ArrowHead	211	3	1	251
Car	120	4	1	577
Coffee	56	2	1	286
GunPoint	200	2	1	150
Herring	128	2	1	512
Lightning2	121	2	1	637
Lightning7	143	7	1	319
Meat	120	3	1	448
OliveOil	60	4	1	570
Rock	70	4	1	2844
SmoothSubspace	300	3	1	15
ToeSegmentation1	268	2	1	277
ToeSegmentation2	166	2	1	343
Trace	200	4	1	275
Wine	111	2	1	234
ArticularWordRecognition	575	25	9	144
BasicMotions	80	4	6	100
CharacterTrajectories	2858	20	3	60-180
Cricket	180	12	6	1197
Epilepsy	275	4	3	206
ERing	300	6	4	65
EthanolConcentration	524	4	3	1751
EyesOpenShut	98	2	14	128
FingerMovements	416	2	28	50
Handwriting	1000	26	3	152
JapaneseVowels	640	9	12	7-26
Libras	360	15	2	45
NATOPS	360	6	24	51
RacketSports	303	4	6	30
SpokenArabicDigits	8798	10	13	4-93

### 4.1 Details of datasets.

We evaluated the proposed framework on a diverse collection of time series datasets from the University of East Anglia (UEA) and the University of California Riverside (UCR) Time Series Classification Repository<sup>1</sup> [1, 15], utilizing the *sktime* Python library [32]. These repositories encompass a wide range of real-world applications, including both univariate and multivariate time series datasets with varying characteristics such as sample size, dimensionality, length, and the number of classes. As summarized in Table 1, we consider 30 different public datasets (15 univariate and 15 multivariate), each divided into three subsets: training, validation, and testing, following a 0.70/0.15/0.15 ratio. To address challenges of varying length time series within the datasets, we employed a uniform scaling approach as recommended by Oh et al. [38].

<sup>1</sup><http://www.timeseriesclassification.com/>

**Data Preprocessing.** Our experiments were conducted on 30 diverse benchmark datasets, following the benchmark protocol established by Oh et al. [38]. For each dataset, we introduced missing observations by randomly removing values, creating a more realistic scenario that mimics real-world data collection challenges, and considered four different missing rates, including regular (0% missing), 30%, 50%, and 70%. Furthermore, to investigate the robustness of the proposed framework, we performed five runs of cross-validation using different random seeds for each run.

**NDE Architecture Design.** As backbone models for the proposed method, we utilize Neural ODE, Neural CDE, and Neural SDE, as explained in Section 3. The vector field of the NDE models consists of nonlinear fully-connected layers with ReLU activation functions. Following the recommendation by Kidger et al. [23], we included Tanh nonlinearity as the final operation for drift, diffusion, and all other vector fields to ensure stability. For all methods, the (explicit) Euler method is employed as the ODE/SDE Solver.

**Hyperparameter optimization.** To automate hyperparameter tuning and minimize validation loss, we utilized the Python library, *ray*<sup>2</sup> [28, 35]. We first identified the best-performing hyperparameters on regular time series and then applied them to the corresponding irregular time series datasets. We employed a combination of search strategies to explore the hyperparameter space. The learning rate  $lr$  was optimized using a log-uniform search in the range of  $10^{-4}$  to  $10^{-1}$ . For the number of layers  $n_l$  in the vector field, we performed a grid search over the set {1, 2, 3, 4}. Similarly, the dimensions of the hidden vectors  $n_h$  were selected from the set {16, 32, 64, 128} using a grid search. The batch size was chosen from the set {16, 32, 64, 128}, striking a balance between memory efficiency and convergence speed.

### 4.2 Comparative Baselines

We evaluated our proposed method against a diverse set of baseline approaches, using their original source code and applying the same hyperparameter tuning procedure described earlier. The baselines can be categorized as follows:

- **Imputation-based methods:** We employed mean imputation for recurrent neural network (RNN) [34, 44], long short-term memory (LSTM) [45], and gated recurrent unit (GRU) [10] models to handle missingness.
- **Temporal feature incorporation:** Following Choi et al. [9] and Che et al. [6], we included models that incorporate additional temporal information, such as GRU- $\Delta t$  and GRU-Simple, which use time gaps and masks as additional inputs. Furthermore, GRU-D utilizes an exponential decay.
- **Attention-based approaches:** We implemented the naive Transformer [50] and enhanced attention-based frameworks such as multi-time attention networks (MTAN) [47] and multi-integration attention module (MIAM) [51] to leverage attention mechanisms.
- **Neural ODE-based methods:** We compared our approach with various neural ODE-based implementations, including GRU-ODE [4], ODE-RNN [42], and ODE-LSTM [25].

<sup>2</sup><https://github.com/ray-project/ray>

**Table 2: Comparative analysis of performance of proposed method and baseline methods on the ‘GunPoint’ dataset. Standard deviations of 5 runs are shown. Bold indicates best performance, underline indicates second-best.**

Category	Method	Regular	Missing Rate			All settings	Proposed method (with TANDEM)		
			30%	50%	70%		Neural ODE	Neural CDE	Neural SDE
Imputation-based	RNN	0.547±0.132	0.480±0.069	0.527±0.166	0.553±0.051	0.527±0.104	20/0/0(*)	20/0/0(*)	20/0/0(*)
	LSTM	0.767±0.156	0.547±0.099	0.513±0.051	0.467±0.058	0.573±0.091	20/0/0(*)	20/0/0(*)	20/0/0(*)
	GRU	0.707±0.196	0.547±0.159	0.547±0.080	0.460±0.043	0.565±0.120	20/0/0(*)	20/0/0(*)	20/0/0(*)
Temporal feature	GRU- $\Delta t$	0.613±0.177	0.607±0.119	0.593±0.064	0.593±0.076	0.602±0.109	20/0/0(*)	20/0/0(*)	20/0/0(*)
	GRU-Simple	0.693±0.095	0.567±0.175	0.487±0.065	0.493±0.028	0.560±0.091	20/0/0(*)	20/0/0(*)	20/0/0(*)
	GRU-D	0.560±0.123	0.613±0.112	0.560±0.083	0.573±0.072	0.577±0.098	20/0/0(*)	20/0/0(*)	20/0/0(*)
Attention-based	Transformer	0.487±0.045	0.487±0.115	0.527±0.104	0.453±0.110	0.488±0.093	20/0/0(*)	20/0/0(*)	20/0/0(*)
	MTAN	0.687±0.102	0.500±0.209	0.573±0.119	0.547±0.096	0.577±0.131	20/0/0(*)	20/0/0(*)	20/0/0(*)
	MIAM	0.540±0.055	0.527±0.080	0.507±0.121	0.533±0.058	0.527±0.078	20/0/0(*)	20/0/0(*)	20/0/0(*)
Neural ODE-based	Neural ODE	0.700±0.094	0.693±0.089	0.693±0.076	0.707±0.055	0.698±0.079	20/0/0(*)	20/0/0(*)	20/0/0(*)
	GRU-ODE	0.913±0.030	0.920±0.051	0.913±0.061	0.920±0.069	0.917±0.053	12/5/3(*)	15/5/0(*)	14/3/3(*)
	ODE-RNN	0.600±0.033	0.587±0.069	0.607±0.136	0.607±0.119	0.600±0.089	20/0/0(*)	20/0/0(*)	20/0/0(*)
	ODE-LSTM	0.633±0.108	0.487±0.018	0.500±0.085	0.540±0.080	0.540±0.073	20/0/0(*)	20/0/0(*)	20/0/0(*)
Neural CDE-based	Neural CDE	0.973±0.028	0.940±0.028	0.947±0.030	0.927±0.043	0.947±0.032	7/9/4	13/7/0(*)	12/4/4
	Neural RDE	0.500±0.062	0.493±0.089	0.493±0.076	0.493±0.089	0.495±0.079	20/0/0(*)	20/0/0(*)	20/0/0(*)
	ANCDE	0.587±0.141	0.693±0.109	0.680±0.135	0.653±0.161	0.653±0.136	19/1/0(*)	19/1/0(*)	19/1/0(*)
	EXIT	0.540±0.196	0.587±0.099	0.507±0.132	0.560±0.148	0.548±0.144	20/0/0(*)	20/0/0(*)	20/0/0(*)
	LEAP	0.460±0.043	0.533±0.085	0.533±0.143	0.580±0.084	0.527±0.089	20/0/0(*)	20/0/0(*)	20/0/0(*)
Neural SDE-based	Neural SDE	0.613±0.130	0.647±0.102	0.673±0.086	0.647±0.150	0.645±0.117	20/0/0(*)	20/0/0(*)	20/0/0(*)
	Neural LSDE	0.893±0.095	0.927±0.060	0.893±0.060	0.873±0.068	0.897±0.071	14/5/1(*)	19/0/1(*)	14/4/2(*)
	Neural LNSDE	0.887±0.084	0.880±0.077	0.887±0.061	0.900±0.075	0.888±0.074	14/5/1(*)	17/3/0(*)	16/1/3(*)
	Neural GSDE	0.853±0.096	0.867±0.062	0.873±0.072	0.873±0.068	0.867±0.075	17/2/1(*)	19/1/0(*)	18/1/1(*)
Proposed	Neural ODE (with TANDEM)	0.973±0.028	0.947±0.018	0.967±0.033	0.960±0.037	0.962±0.029	-	10/8/2(*)	8/3/9
	Neural CDE (with TANDEM)	0.987±0.018	0.987±0.018	0.980±0.030	0.967±0.024	0.980±0.022	2/8/10	-	4/6/10
	Neural SDE (with TANDEM)	0.973±0.015	0.980±0.045	0.973±0.028	0.933±0.033	0.965±0.030	9/3/8	10/6/4(*)	-

- Neural CDE-based approaches:** We used the original Neural CDE with Hermite cubic splines [23], Neural RDE with depth 2 signature transform and cubic interpolation. Additional to that, ANCDE [22], EXIT (EXtrapolation and InTerpolation) [21], and LEAP (LEArnable Path) [20] are included.
- Neural SDE-based methods:** We considered statistically stable Neural SDEs proposed by Oh et al. [38]: Neural Langevin-type SDE (LSDE), Neural Linear Noise SDE (LNSDE), and Neural Geometric SDE (GSDE). These models combine control path into the augmented states.

### 4.3 Case Study: ‘GunPoint’ Dataset

The ‘GunPoint’ dataset, introduced by Ratanamahatana and Keogh [40], is a binary classification problem in time series analysis. It consists of motion data from two actors (one female, one male) performing two distinct hand movements: Gun-Draw and Point. The dataset tracks the X-axis movement of the actors’ right hands, capturing the temporal dynamics of these actions. To further illustrate the effectiveness of our proposed TANDEM framework, we conducted a detailed case study, under four different settings.

Our TANDEM framework demonstrates robust performance across all settings, maintaining high accuracy even with significant portions of missing data, as represented in Table 2. When missing rates are increased, the benchmark’s performance degrades, while our model remains impressively high accuracy. The integration of TANDEM yields performance improvements across all baselines. We observe significant enhancements in Neural ODE and Neural SDE, whereas the improvements in Neural CDE are more moderate.

To rigorously assess performance differences between TANDEM and baseline methods, we employ the one-sided Wilcoxon signed-rank test [11], suitable for comparing paired results on the same

dataset. To account for multiple comparisons, we apply the Holm-Bonferroni correction [14], using a corrected significance threshold of  $p < 0.05$  in line with best practices [3]. We analyze ‘GunPoint’ dataset individually across four missing rates (0%, 30%, 50%, 70%), with five repetitions per condition, yielding 20 paired observations per model. In the right panel of Table 2, our framework clearly outperforms the baseline methods, with Neural CDE being the strongest competitor. However, our approach (Neural CDE with TANDEM) achieves a slight improvement even over this strong baseline. Although this single-dataset analysis provides useful insights, its generalizability is limited. To address this, we extend our experiments to a broader set of datasets as represented in Table 1.

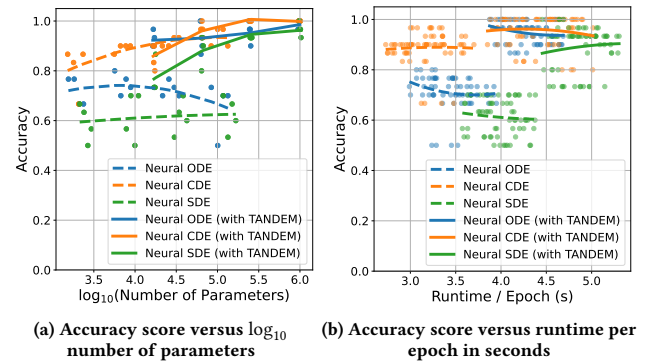


**Figure 2: Performance-computation trade-off analysis with NDE baselines and their TANDEM variants. Each point reflects a model with different layer counts ( $n_l$ ) and hidden sizes ( $n_h$ ). Dashed/Solid lines show second-order polynomial trends for each model family. Each configuration is repeated five times.**

**Table 3: Classification performance on 30 benchmark datasets with regular and three missing rates. The values within the parentheses indicate the average of individual standard deviations. (\*) denotes statistically significant superiority of pairwise comparison (Win/Tie/Loss counts) and one-sided Wilcoxon signed-rank test with  $p < 0.05$**

Method	Regular		30% Missing		50% Missing		70% Missing		All settings		Proposed method (with TANDEM)		
	Accuracy	Rank	Neural ODE	Neural CDE	Neural SDE								
RNN	0.582 (0.064)	18.42	0.513 (0.087)	20.12	0.485 (0.088)	21.70	0.472 (0.072)	20.58	0.513 (0.078)	20.20	114/1/5(*)	113/2/5(*)	114/0/6(*)
LSTM	0.633 (0.053)	15.40	0.595 (0.060)	16.33	0.567 (0.061)	17.15	0.558 (0.058)	16.60	0.589 (0.058)	16.37	99/6/15(*)	104/0/16(*)	108/0/12(*)
GRU	0.672 (0.059)	11.45	0.621 (0.063)	13.77	0.610 (0.055)	13.97	0.597 (0.062)	13.78	0.625 (0.060)	13.24	81/3/36(*)	90/2/28(*)	85/4/31(*)
GRU- $\Delta t$	0.641 (0.070)	14.00	0.636 (0.066)	12.37	0.634 (0.056)	11.93	0.618 (0.065)	13.75	0.632 (0.064)	13.01	81/4/35(*)	85/2/33(*)	84/5/31(*)
GRU-Simple	0.669 (0.060)	11.38	0.640 (0.063)	11.55	0.613 (0.071)	13.62	0.569 (0.072)	15.78	0.623 (0.066)	13.08	83/3/34(*)	86/1/33(*)	85/1/34(*)
GRU-D	0.648 (0.071)	14.32	0.624 (0.075)	14.35	0.611 (0.073)	15.07	0.604 (0.067)	14.38	0.622 (0.072)	14.53	93/0/27(*)	98/4/18(*)	92/3/25(*)
Transformer	0.664 (0.069)	13.52	0.625 (0.068)	15.05	0.627 (0.061)	14.97	0.607 (0.066)	15.02	0.631 (0.066)	14.64	90/4/26(*)	92/1/27(*)	96/2/22(*)
MTAN	0.648 (0.080)	16.42	0.618 (0.099)	14.80	0.618 (0.091)	13.82	0.607 (0.078)	13.30	0.623 (0.087)	14.58	97/1/22(*)	102/1/17(*)	96/1/23(*)
MIAM	0.623 (0.048)	14.88	0.603 (0.066)	14.92	0.589 (0.063)	16.58	0.569 (0.056)	16.38	0.596 (0.058)	15.69	95/3/22(*)	99/2/19(*)	93/4/23(*)
Neural ODE	0.521 (0.065)	18.70	0.518 (0.061)	17.47	0.515 (0.060)	17.22	0.526 (0.058)	16.28	0.520 (0.061)	17.42	112/3/5(*)	109/0/11(*)	108/5/7(*)
GRU-ODE	0.671 (0.067)	13.72	0.663 (0.064)	13.23	0.664 (0.059)	11.52	0.655 (0.064)	11.22	0.664 (0.063)	12.42	93/1/26(*)	96/2/22(*)	86/1/33(*)
ODE-RNN	0.658 (0.063)	12.73	0.635 (0.064)	13.13	0.636 (0.067)	11.38	0.630 (0.055)	11.55	0.640 (0.062)	12.20	87/3/30(*)	90/3/27(*)	83/5/32(*)
ODE-LSTM	0.619 (0.063)	15.42	0.584 (0.064)	16.30	0.561 (0.065)	17.60	0.530 (0.085)	17.20	0.574 (0.069)	16.63	99/3/18(*)	105/0/15(*)	102/3/15(*)
Neural CDE	0.709 (0.061)	12.03	0.706 (0.073)	9.47	0.696 (0.064)	9.42	0.665 (0.072)	10.93	0.694 (0.068)	10.46	75/5/40(*)	88/6/26(*)	76/3/41(*)
Neural RDE	0.678 (0.066)	13.02	0.658 (0.074)	12.57	0.640 (0.067)	13.65	0.626 (0.077)	12.33	0.651 (0.071)	12.89	83/4/33(*)	95/4/21(*)	85/1/34(*)
ANCDE	0.693 (0.067)	11.23	0.687 (0.068)	10.60	0.683 (0.078)	9.82	0.655 (0.067)	10.07	0.679 (0.070)	10.43	74/2/44(*)	89/4/27(*)	77/3/40(*)
EXIT	0.636 (0.073)	15.37	0.633 (0.078)	14.60	0.616 (0.075)	14.68	0.599 (0.075)	15.28	0.621 (0.075)	14.98	103/2/15(*)	106/1/13(*)	105/1/14(*)
LEAP	0.444 (0.068)	19.60	0.401 (0.078)	21.07	0.425 (0.073)	19.35	0.414 (0.070)	19.73	0.421 (0.072)	19.94	115/0/5(*)	113/0/7(*)	111/1/8(*)
Neural SDE	0.526 (0.068)	17.77	0.508 (0.066)	17.67	0.517 (0.058)	17.68	0.512 (0.066)	17.68	0.516 (0.064)	17.70	109/0/11(*)	106/1/13(*)	107/1/12(*)
Neural LSDE	0.717 (0.056)	7.93	0.690 (0.050)	9.23	0.686 (0.051)	8.72	0.682 (0.067)	7.30	0.694 (0.056)	8.30	62/8/50(*)	72/3/45(*)	61/11/48(*)
Neural LNSDE	0.727 (0.047)	7.98	0.723 (0.050)	7.48	0.717 (0.054)	6.20	0.703 (0.054)	6.13	0.717 (0.051)	6.95	59/6/55	60/4/56	52/6/62
Neural GSDE	0.716 (0.065)	8.22	0.707 (0.069)	8.02	0.698 (0.063)	8.43	0.689 (0.056)	7.67	0.703 (0.063)	8.08	59/8/53	71/4/45(*)	59/7/54
Neural ODE (with TANDEM)	0.738 (0.055)	8.70	0.737 (0.063)	6.67	0.737 (0.060)	6.52	0.700 (0.067)	7.62	0.728 (0.061)	7.38	-	65/3/52	51/11/58
Neural CDE (with TANDEM)	0.767 (0.053)	5.87	0.750 (0.051)	6.58	0.742 (0.062)	6.37	0.709 (0.064)	6.83	0.742 (0.057)	6.41	52/3/65	-	48/2/70
Neural SDE (with TANDEM)	0.749 (0.058)	6.93	0.724 (0.054)	7.67	0.713 (0.060)	7.65	0.696 (0.051)	7.58	0.721 (0.056)	7.46	58/11/51	70/2/48(*)	-

For further analysis, we examine the performance–computation trade-off of our proposed method, as shown in Figure 2. Note that computational time is largely influenced by the choice of solver [38]. Specifically, we used *torchcde*<sup>3</sup> [23] for Neural CDEs, and *torchsde*<sup>4</sup> [27] for Neural ODEs and SDEs.

Figure 2 (a) and (b) together illustrate the trade-off between accuracy and computation. While Figure 2 (a) shows that TANDEM improves parameter efficiency by achieving higher accuracy with comparable model sizes, Figure 2 (b) reveals the cost: TANDEM variants consistently require longer runtimes per epoch due to added attention and gating overhead. This highlights a key trade-off between predictive performance and computational efficiency.

#### 4.4 Comprehensive results on 30 Datasets

Table 3 compares the classification accuracy over five iterations. We observe that TANDEM maintains relatively stable performance across all tested scenarios, in contrast to most baselines that degrade noticeably under higher missingness. This stability suggests that the proposed incorporation of explicit features provides a robust mechanism for recovering meaningful temporal dynamics, even in situations where large fractions of the data are unobserved.

For a broader comparison, we average results over five runs for each of the 30 datasets and four missing rates, generating 120 data points per method. These are used for pairwise tests and corrected  $p$ -values, offering a more robust evaluation across diverse datasets. The number of pairwise comparisons (including Win/Tie/Loss counts) and statistical test results are summarized in the right panel of Table 3. For instance, Neural CDE with TANDEM achieves the best average rank across all missingness settings.

<sup>3</sup><https://github.com/patrick-kidger/torchcde>

<sup>4</sup><https://github.com/google-research/torchsde>

The Win/Tie/Loss counts further highlight the TANDEM framework’s effectiveness, showing numerous statistically significant wins against other approaches. When compared to Neural LNSDE, our method achieves more wins in one-to-one comparisons, although the difference is not statistically significant.

**Table 4: Average value of the proposed gate activations on 30 benchmark datasets for varying missing rates (The values within the parentheses indicate the average of individual standard deviations.)**

Neural ODE (with TANDEM)	Regular	Missing Rate		
		30%	50%	70%
$\sigma_{\hat{x}}$	0.473 (0.393)	0.513 (0.424)	0.447 (0.411)	0.473 (0.357)
$\sigma_x$	0.533 (0.408)	0.520 (0.386)	0.580 (0.351)	0.527 (0.413)
$\sigma_z$	0.880 (0.111)	0.853 (0.158)	0.873 (0.118)	0.867 (0.192)

Neural CDE (with TANDEM)	Regular	Missing Rate		
		30%	50%	70%
$\sigma_{\hat{x}}$	0.340 (0.353)	0.307 (0.365)	0.273 (0.342)	0.307 (0.443)
$\sigma_x$	0.187 (0.270)	0.233 (0.376)	0.220 (0.277)	0.280 (0.365)
$\sigma_z$	0.720 (0.396)	0.713 (0.345)	0.680 (0.398)	0.707 (0.353)

Neural SDE (with TANDEM)	Regular	Missing Rate		
		30%	50%	70%
$\sigma_{\hat{x}}$	0.533 (0.340)	0.487 (0.372)	0.500 (0.313)	0.447 (0.395)
$\sigma_x$	0.487 (0.309)	0.527 (0.365)	0.533 (0.317)	0.527 (0.353)
$\sigma_z$	0.867 (0.144)	0.847 (0.169)	0.833 (0.194)	0.853 (0.166)

Furthermore, the results show that our attention-guided framework significantly improves performance for both neural ODE and SDE models compared to their naïve approaches. Neural CDE shows modest performance gains with proposed method since it already incorporates control paths in its formulation. Nevertheless, Neural

CDE with TANDEM achieves the highest accuracy across all scenarios. This improvement supports our hypothesis that incorporating complementary inputs through attention mechanisms can enhance the model's ability to handle missing data in time series.

Table 4 presents the average gating values  $\sigma_{\tilde{x}}$ ,  $\sigma_X$ , and  $\sigma_z$  across 30 datasets and various missing rates. While each individual gate is drawn from a near-binary Gumbel-Sigmoid distribution at the level of a single sample and time step, the table reports averages over large collections of runs.

A key takeaway is that when missingness is moderate to high,  $\sigma_X$  and  $\sigma_z$  often increase, suggesting that the gating mechanism elevates interpolation or latent trajectory in regions of sparse or noisy measurements. Conversely, at lower missing rates,  $\sigma_{\tilde{x}}$  remains non-trivial, indicating that direct observations provide a concrete information whenever they are sufficiently present. In conclusion, these average gate values align well with the intuition that TANDEM adaptively allocates more weight to the control path or latent dynamics when raw data are unreliable, yet reverts to directly using raw measurements when they are abundant and trustworthy.

## 4.5 Ablation Study

**Table 5: Ablation study on 30 benchmark datasets with regular and three missing rates (The values within the parentheses indicate the average of individual standard deviations.)**

Component	Regular	Missing Rate			All Settings
		30%	50%	70%	
TANDEM	0.738 (0.055)	0.737 (0.063)	0.737 (0.060)	0.700 (0.067)	0.728 (0.061)
TANDEM (soft)	0.706 (0.063)	0.701 (0.075)	0.681 (0.071)	0.671 (0.066)	0.690 (0.068)
$[\Phi_{z(t)}, \Phi_{\tilde{x}(t)}, \Phi_{X(t)}]$	0.701 (0.063)	0.687 (0.067)	0.670 (0.073)	0.652 (0.072)	0.677 (0.069)
$[\Phi_{z(t)}, \Phi_{X(t)}]$	0.710 (0.063)	0.701 (0.068)	0.690 (0.080)	0.673 (0.070)	0.694 (0.070)
$[\Phi_{z(t)}, \Phi_{\tilde{x}(t)}]$	0.688 (0.069)	0.681 (0.075)	0.658 (0.072)	0.636 (0.078)	0.666 (0.073)
$\Phi_{z(t)}$ only	0.519 (0.074)	0.520 (0.060)	0.516 (0.064)	0.525 (0.062)	0.520 (0.065)
w/o attention	0.521 (0.065)	0.518 (0.061)	0.515 (0.060)	0.526 (0.058)	0.520 (0.061)
TANDEM	0.767 (0.053)	0.750 (0.051)	0.742 (0.062)	0.709 (0.064)	0.742 (0.057)
TANDEM (soft)	0.751 (0.057)	0.737 (0.063)	0.722 (0.065)	0.692 (0.070)	0.726 (0.063)
$[\Phi_{z(t)}, \Phi_{\tilde{x}(t)}, \Phi_{X(t)}]$	0.720 (0.057)	0.714 (0.071)	0.708 (0.066)	0.684 (0.068)	0.707 (0.066)
$[\Phi_{z(t)}, \Phi_{X(t)}]$	0.711 (0.059)	0.710 (0.067)	0.692 (0.058)	0.677 (0.066)	0.697 (0.062)
$[\Phi_{z(t)}, \Phi_{\tilde{x}(t)}]$	0.741 (0.055)	0.727 (0.060)	0.703 (0.075)	0.681 (0.064)	0.713 (0.064)
$\Phi_{z(t)}$ only	0.724 (0.073)	0.707 (0.055)	0.702 (0.067)	0.684 (0.063)	0.705 (0.065)
w/o attention	0.709 (0.061)	0.706 (0.073)	0.696 (0.064)	0.665 (0.064)	0.694 (0.068)
TANDEM	0.749 (0.058)	0.724 (0.054)	0.713 (0.060)	0.696 (0.051)	0.721 (0.056)
TANDEM (soft)	0.718 (0.067)	0.689 (0.060)	0.677 (0.063)	0.659 (0.066)	0.686 (0.064)
$[\Phi_{z(t)}, \Phi_{\tilde{x}(t)}, \Phi_{X(t)}]$	0.709 (0.051)	0.689 (0.063)	0.669 (0.072)	0.657 (0.061)	0.681 (0.062)
$[\Phi_{z(t)}, \Phi_{X(t)}]$	0.677 (0.078)	0.663 (0.076)	0.655 (0.070)	0.655 (0.060)	0.662 (0.071)
$[\Phi_{z(t)}, \Phi_{\tilde{x}(t)}]$	0.687 (0.067)	0.656 (0.071)	0.645 (0.075)	0.637 (0.071)	0.656 (0.071)
$\Phi_{z(t)}$ only	0.524 (0.059)	0.523 (0.068)	0.520 (0.063)	0.524 (0.068)	0.523 (0.064)
w/o attention	0.526 (0.068)	0.508 (0.066)	0.517 (0.058)	0.512 (0.066)	0.516 (0.064)

We evaluated the performance of the framework using various combinations of attention components, including raw observation

$\tilde{x}(t)$ , control path  $X(t)$ , and continuous latent dynamics  $z(t)$ . We also considered soft method without hard thresholding in the attention gating module. The naïve approach, which did not include any attention mechanism, served as a baseline for comparison in Table 5. Overall, TANDEM framework improves the performance across various benchmark datasets with missing values.

Figure 3 then summarizes an ablation study, showing how different feature components affect performance. We observe that removing attention or restricting the model to a single feature yields a drop in accuracy across all missing rates, confirming the importance of multi-feature integration. Variations of the model that only leverage one feature exhibit higher variance and reduced accuracy, particularly at moderate to high missing rates. In contrast, the full TANDEM framework with multi-head attention and gating consistently yields narrower box plots, reflecting lower variance and higher median accuracy.

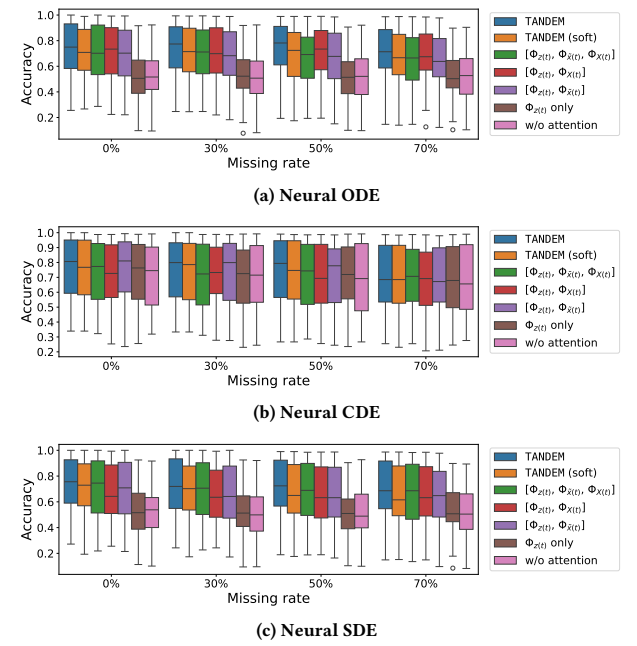


**Figure 3: Ablation study regarding model configuration**

## 5 Real-world data analysis

To evaluate the effectiveness of our proposed TANDEM framework in a real-world scenario, we conducted an additional study using a medical dataset, ‘PhysioNet Sepsis’. The 2019 PhysioNet / Computing in Cardiology (CinC) challenge on Sepsis prediction serves as the foundation for time-series classification experiments [41]. The dataset used in these experiments contains 40,335 cases of patients admitted to intensive care units, with 34 time-dependent variables such as heart rate, oxygen saturation, and body temperature. The primary objective is to classify whether each patient has sepsis or not according to the sepsis-3 definition.

*Experimental Setup.* The PhysioNet dataset is an irregular time series dataset, as only 10% of the values are sampled with their

respective timestamps for each patient. To address this irregularity, two types of time-series classification are performed: (OI) classification using observation intensity, and (no OI) classification without using observation intensity. In medical context, observation intensity is a measure of the degree of illness, and when incorporated, an index number is appended to each value in the time series.

## 5.1 Results analysis

Given the data's imbalanced nature, we evaluate performance using the Area Under the Receiver Operating Characteristic (AUROC) score. We used the reported performance from Jhin et al. [22] and Oh et al. [38] to compare with our method. In Table 6, our TANDEM framework demonstrated robust performance in both OI and no OI settings. The incorporation of observation intensity generally improved the classification performance, indicating the importance of explicit features. These results underscore the potential of our TANDEM framework in real-world medical applications.

**Table 6: AUROC on PhysioNet Sepsis**

Method	Test AUROC	
	OI	No OI
GRU- $\Delta t$	0.878 $\pm$ 0.006	0.840 $\pm$ 0.007
GRU-D	0.871 $\pm$ 0.022	0.850 $\pm$ 0.013
GRU-ODE	0.852 $\pm$ 0.010	0.771 $\pm$ 0.024
ODE-RNN	0.874 $\pm$ 0.016	0.833 $\pm$ 0.020
Latent-ODE	0.787 $\pm$ 0.011	0.495 $\pm$ 0.002
ACE-NODE	0.804 $\pm$ 0.010	0.514 $\pm$ 0.003
Neural CDE	0.880 $\pm$ 0.006	0.776 $\pm$ 0.009
ANCDE	0.900 $\pm$ 0.002	0.823 $\pm$ 0.003
EXIT	0.913 $\pm$ 0.002	0.836 $\pm$ 0.003
Neural LSDE	0.909 $\pm$ 0.004	0.879 $\pm$ 0.008
Neural LNSDE	0.911 $\pm$ 0.002	0.881 $\pm$ 0.002
Neural GSDE	0.909 $\pm$ 0.001	0.884 $\pm$ 0.002
<b>Neural ODE (with TANDEM)</b>	<b>0.916<math>\pm</math>0.005</b>	0.877 $\pm$ 0.008
<b>Neural CDE (with TANDEM)</b>	0.909 $\pm$ 0.006	<b>0.893<math>\pm</math>0.003</b>
<b>Neural SDE (with TANDEM)</b>	0.913 $\pm$ 0.005	0.873 $\pm$ 0.004

Moreover, our findings support the hypothesis that missing data patterns can contribute to a deeper understanding of time series. While attention applied to learned latent features shows marginal improvements, incorporating attention on raw observation or on the control path leads to more substantial performance gains. This indicates that missingness patterns encode predictive signals, offering useful context beyond the observed values themselves.

**Table 7: Average gate activations on PhysioNet Sepsis**

Model Component	OI	No OI
Neural ODE (with TANDEM)	$\sigma_{\tilde{x}}$	0.600 $\pm$ 0.548
	$\sigma_X$	0.600 $\pm$ 0.548
	$\sigma_z$	1.000 $\pm$ 0.000
Neural CDE (with TANDEM)	$\sigma_{\tilde{x}}$	0.400 $\pm$ 0.548
	$\sigma_X$	0.000 $\pm$ 0.000
	$\sigma_z$	1.000 $\pm$ 0.000
Neural SDE (with TANDEM)	$\sigma_{\tilde{x}}$	0.800 $\pm$ 0.447
	$\sigma_X$	1.000 $\pm$ 0.000
	$\sigma_z$	1.000 $\pm$ 0.000

Table 7 summarizes the average gate activations under two conditions. The latent gate  $\sigma_z$  maintains consistently high values, indicating the importance of learned continuous-time dynamics. The gates  $\sigma_{\tilde{x}}$  and  $\sigma_X$  show moderate values that adapt based on the presence of observation intensity features, while preserving the

model's reliance on its continuous-time backbone. Overall, the proposed Gumbel-Sigmoid gating behavior confirms TANDEM's flexibility in utilizing the most informative features across different data scenarios.

## 5.2 Ablation study

To assess the efficacy of our approach, we conducted a comprehensive ablation study, with results presented in Table 8. This analysis reveals that the TANDEM framework consistently improves the performance of NDE-based models compared to their respective baselines. These enhancements highlight the effectiveness of our proposed attention-guided mechanism in addressing the complexities of time series data.

**Table 8: Ablation study on PhysioNet Sepsis**

Baseline	Component	Test AUROC	
		OI	No OI
Neural ODE	TANDEM	0.916 $\pm$ 0.005	0.877 $\pm$ 0.008
	TANDEM (soft)	0.898 $\pm$ 0.007	0.860 $\pm$ 0.012
	$[\Phi_{z(t)}, \Phi_{\tilde{x}(t)}, \Phi_X(t)]$	0.912 $\pm$ 0.007	0.864 $\pm$ 0.009
	$[\Phi_{z(t)}, \Phi_X(t)]$	0.911 $\pm$ 0.004	0.868 $\pm$ 0.020
	$[\Phi_{z(t)}, \Phi_{\tilde{x}(t)}]$	0.909 $\pm$ 0.004	0.848 $\pm$ 0.005
	$\Phi_{z(t)}$ only	0.849 $\pm$ 0.012	0.846 $\pm$ 0.005
Neural CDE	w/o attention	0.844 $\pm$ 0.008	0.851 $\pm$ 0.006
	TANDEM	0.909 $\pm$ 0.006	0.893 $\pm$ 0.003
	TANDEM (soft)	0.896 $\pm$ 0.005	0.885 $\pm$ 0.005
	$[\Phi_{z(t)}, \Phi_{\tilde{x}(t)}, \Phi_X(t)]$	0.892 $\pm$ 0.003	0.887 $\pm$ 0.004
	$[\Phi_{z(t)}, \Phi_X(t)]$	0.902 $\pm$ 0.005	0.885 $\pm$ 0.003
	$[\Phi_{z(t)}, \Phi_{\tilde{x}(t)}]$	0.904 $\pm$ 0.003	0.889 $\pm$ 0.006
Neural SDE	$\Phi_{z(t)}$ only	0.907 $\pm$ 0.008	0.886 $\pm$ 0.005
	w/o attention	0.888 $\pm$ 0.002	0.864 $\pm$ 0.005
	TANDEM	0.913 $\pm$ 0.005	0.873 $\pm$ 0.004
	TANDEM (soft)	0.909 $\pm$ 0.003	0.853 $\pm$ 0.013
	$[\Phi_{z(t)}, \Phi_{\tilde{x}(t)}, \Phi_X(t)]$	0.911 $\pm$ 0.007	0.861 $\pm$ 0.006
	$[\Phi_{z(t)}, \Phi_X(t)]$	0.903 $\pm$ 0.006	0.872 $\pm$ 0.006
	$[\Phi_{z(t)}, \Phi_{\tilde{x}(t)}]$	0.902 $\pm$ 0.009	0.847 $\pm$ 0.005
	$\Phi_{z(t)}$ only	0.846 $\pm$ 0.008	0.846 $\pm$ 0.006
	w/o attention	0.850 $\pm$ 0.004	0.848 $\pm$ 0.003

The improved AUROC scores achieved by our TANDEM framework on the PhysioNet Sepsis dataset suggest that it can effectively aid in early detection of sepsis, potentially leading to timely interventions and improved patient outcomes. Our method can be valuable in healthcare and clinical settings where data collection is often incomplete or irregular.

## 6 Conclusion

We introduced a novel attention-guided NDE framework for time series classification in the presence of missing values. Our approach combines the strengths of attention mechanisms and neural differential equations to capture the underlying dynamics of incomplete time series data and improve classification performance. Integrating attention mechanisms with NDEs enables a more robust and accurate classification of time series containing missing values.

While our framework demonstrates significant improvements, it also presents certain limitations. The computational complexity of training NDEs with attention mechanisms can be high, especially for large-scale datasets. Future research could explore more efficient training algorithms or approximation methods to address scalability. Additionally, extending the framework to other tasks, and investigating its performance under different missingness mechanisms, are promising directions for further study.

## Acknowledgments

This research was supported by the Basic Science Research Program through the National Research Foundation of Korea (NRF) funded by the Ministry of Education (RS-2024-00407852); the Korea Health Technology R&D Project through the Korea Health Industry Development Institute (KHIDI), funded by the Ministry of Health and Welfare, Republic of Korea (HI19C1095); the Ministry of Trade, Industry and Energy (MOTIE) and Korea Institute for Advancement of Technology (KIAT) through the International Cooperative R&D program (No.P0025828); Institute of Information & communications Technology Planning & Evaluation (IITP) grant funded by the Korea government (MSIT) (No. RS-2020-II201336, Artificial Intelligence Graduate School Program (UNIST)); and the National Research Foundation of Korea (NRF) grant funded by the Korea government (MSIT) (RS-2025-00563597).

## GenAI Usage Disclosure

We used Generative AI tools (e.g., large language models) solely for language editing and rephrasing. No AI-generated content was used to propose novel ideas, or conduct experiments. All intellectual contributions are solely those of the authors.

## References

- [1] Anthony Bagnall, Hoang Anh Dau, Jason Lines, Michael Flynn, James Large, Aaron Bostrom, Paul Southam, and Eamonn Keogh. 2018. The UEA multivariate time series classification archive, 2018. <https://doi.org/10.48550/ARXIV.1811.00075>
- [2] Dzmitry Bahdanau, Kyunghyun Cho, and Yoshua Bengio. 2015. Neural Machine Translation by Jointly Learning to Align and Translate.. In *3rd International Conference on Learning Representations, ICLR 2015, San Diego, CA, USA, May 7-9, 2015, Conference Track Proceedings*.
- [3] Alessio Benavoli, Giorgio Corani, and Francesca Mangili. 2016. Should We Really Use Post-Hoc Tests Based on Mean-Ranks? *Journal of Machine Learning Research* 17, 5 (2016), 1–10.
- [4] Edward De Brouwer, Jaak Simm, Adam Arany, and Yves Moreau. 2019. GRU-ODE-Bayes: Continuous Modeling of Sporadically-Observed Time Series.. In *Advances in Neural Information Processing Systems 32: Annual Conference on Neural Information Processing Systems 2019, NeurIPS 2019, December 8-14, 2019, Vancouver, BC, Canada*. 7377–7388.
- [5] Wei Cao, Dong Wang, Jian Li, Hao Zhou, Lei Li, and Yitan Li. 2018. BRITS: Bidirectional Recurrent Imputation for Time Series.. In *Advances in Neural Information Processing Systems 31: Annual Conference on Neural Information Processing Systems 2018, NeurIPS 2018, December 3-8, 2018, Montréal, Canada*. 6776–6786.
- [6] Zhengping Che, Sanjay Purushotham, Kyunghyun Cho, David Sontag, and Yan Liu. 2018. Recurrent Neural Networks for Multivariate Time Series with Missing Values. *Scientific Reports* 8, 1 (April 2018), 6085. <https://doi.org/10.1038/s41598-018-24271-9>
- [7] Tian Qi Chen, Yulia Rubanova, Jesse Bettencourt, and David Duvenaud. 2018. Neural Ordinary Differential Equations.. In *Advances in Neural Information Processing Systems 31: Annual Conference on Neural Information Processing Systems 2018, NeurIPS 2018, December 3-8, 2018, Montréal, Canada*. 6572–6583.
- [8] Yuqi Chen, Kan Ren, Yansen Wang, Yuchen Fang, Weiwei Sun, and Dongsheng Li. 2023. ContiFormer: continuous-time transformer for irregular time series modeling. In *Proceedings of the 37th International Conference on Neural Information Processing Systems (NIPS '23)*. Curran Associates Inc., Red Hook, NY, USA.
- [9] Edward Choi, Mohammad Taha Bahadori, Andy Schuetz, Walter F. Stewart, and Jimeng Sun. 2016. Doctor AI: Predicting Clinical Events via Recurrent Neural Networks. In *Proceedings of the 1st Machine Learning for Healthcare Conference (Proceedings of Machine Learning Research, Vol. 56)*. Finale Doshi-Velez, Jim Fackler, David Kale, Byron Wallace, and Jenna Wiens (Eds.). PMLR, Northeastern University, Boston, MA, USA, 301–318.
- [10] Junyoung Chung, Caglar Gulcehre, KyungHyun Cho, and Yoshua Bengio. 2014. Empirical Evaluation of Gated Recurrent Neural Networks on Sequence Modeling. <https://doi.org/10.48550/ARXIV.1412.3555>
- [11] Janez Demšar. 2006. Statistical Comparisons of Classifiers over Multiple Data Sets. *J. Mach. Learn. Res.* 7 (Dec. 2006), 1–30.
- [12] Emilian Dupont, Arnaud Doucet, and Yee Whye Teh. 2019. Augmented Neural ODEs.. In *Advances in Neural Information Processing Systems 32: Annual Conference on Neural Information Processing Systems 2019, NeurIPS 2019, December 8-14, 2019, Vancouver, BC, Canada*. 3134–3144.
- [13] Tlalelo Emmanuel, Thabiso Maupong, Dimane MpoeLeng, Thabo Semong, Banyatsang Mphago, and Oteng Tabona. 2021. A survey on missing data in machine learning. *Journal of Big Data* 8, 1 (Oct. 2021), 140. <https://doi.org/10.1186/s40537-021-00516-9>
- [14] Massimiliano Giacalone, Zirilli Agata, Paolo Carmelo Cozzuoli, and Angela Alibrandi. 2018. Bonferroni-Holm and permutation tests to compare health data: methodological and applicative issues. *BMC Medical Research Methodology* 18, 1 (July 2018), 81. <https://doi.org/10.1186/s12874-018-0540-8>
- [15] H. A. Dau, A. Bagnall, K. Kamgar, C. -C. M. Yeh, Y. Zhu, S. Gharghabi, C. A. Ratanamahatana, and E. Keogh. 2019. The UCR time series archive. *IEEE/CAA Journal of Automatica Sinica* 6, 6 (Nov. 2019), 1293–1305. <https://doi.org/10.1109/JAS.2019.1911747>
- [16] J. -T. Chien and Y. -H. Chen. 2021. Continuous-Time Self-Attention in Neural Differential Equation. In *ICASSP 2021 - 2021 IEEE International Conference on Acoustics, Speech and Signal Processing (ICASSP)*. 3290–3294. <https://doi.org/10.1109/ICASSP39728.2021.9414104>
- [17] Eric Jang, Shixiang Gu, and Ben Poole. 2017. Categorical Reparameterization with Gumbel-Softmax. In *5th International Conference on Learning Representations, ICLR 2017, Toulon, France, April 24-26, 2017, Conference Track Proceedings*.
- [18] Kristel J.M. Janssen, A. Rogier T. Donders, Frank E. Harrell, Yvonne Vergouwe, Qingxia Chen, Diederick E. Grobbee, and Karel G.M. Moons. 2010. Missing covariate data in medical research: To impute is better than to ignore. *Journal of Clinical Epidemiology* 63, 7 (July 2010), 721–727. <https://doi.org/10.1016/j.jclinepi.2009.12.008>
- [19] Sheo Yon Jhin, Minju Jo, Taeyong Kong, Jinsung Jeon, and Noseong Park. 2021. ACE-NODE: Attentive Co-Evolving Neural Ordinary Differential Equations. In *Proceedings of the 27th ACM SIGKDD Conference on Knowledge Discovery & Data Mining (KDD '21)*. Association for Computing Machinery, New York, NY, USA, 736–745. <https://doi.org/10.1145/3447548.3467419>
- [20] Sheo Yon Jhin, Minju Jo, Seungji Kook, and Noseong Park. 2023. Learnable Path in Neural Controlled Differential Equations. *Proceedings of the AAAI Conference on Artificial Intelligence* 37, 7 (June 2023), 8014–8022. <https://doi.org/10.1609/aaai.v37i7.25969>
- [21] Sheo Yon Jhin, Jaehoon Lee, Minju Jo, Seungji Kook, Jinsung Jeon, Jihyeon Hyeong, Jayoung Kim, and Noseong Park. 2022. EXIT: Extrapolation and Interpolation-based Neural Controlled Differential Equations for Time-series Classification and Forecasting.. In *WWW '22: The ACM Web Conference 2022, Virtual Event, Lyon, France, April 25 - 29, 2022*. 3102–3112. <https://doi.org/10.1145/3485447.3512030>
- [22] Sheo Yon Jhin, Heejoo Shin, Sujei Kim, Seoyoung Hong, Minju Jo, Solhee Park, Noseong Park, Seungbeom Lee, Hwiyoung Maeng, and Seungmin Jeon. 2024. Attentive neural controlled differential equations for time-series classification and forecasting. *Knowledge and Information Systems* 66, 3 (March 2024), 1885–1915. <https://doi.org/10.1007/s10115-023-01977-5>
- [23] Patrick Kidger, James Morrill, James Foster, and Terry J. Lyons. 2020. Neural Controlled Differential Equations for Irregular Time Series.. In *Advances in Neural Information Processing Systems 33: Annual Conference on Neural Information Processing Systems 2020, NeurIPS 2020, December 6-12, 2020, virtual*.
- [24] Diederik P. Kingma and Jimmy Ba. 2015. Adam: A Method for Stochastic Optimization. In *3rd International Conference on Learning Representations, ICLR 2015, San Diego, CA, USA, May 7-9, 2015, Conference Track Proceedings*. Yoshua Bengio and Yann LeCun (Eds.).
- [25] Mathias Lechner and Ramin Hasani. 2020. Learning Long-Term Dependencies in Irregularly-Sampled Time Series. <https://doi.org/10.48550/arXiv.2006.04418>
- [26] Bei Li, Quan Du, Tao Zhou, Yi Jing, Shuhua Zhou, Xin Zeng, Tong Xiao, JingBo Zhu, Xuebo Liu, and Min Zhang. 2022. ODE Transformer: An Ordinary Differential Equation-Inspired Model for Sequence Generation. In *Proceedings of the 60th Annual Meeting of the Association for Computational Linguistics (Volume 1: Long Papers)*. Smaranda Muresan, Preslav Nakov, and Aline Villavicencio (Eds.). Association for Computational Linguistics, Dublin, Ireland, 8335–8351. <https://doi.org/10.18653/v1/2022.acl-long.571>
- [27] Xuechen Li, Ting-Kam Leonard Wong, Ricky T. Q. Chen, and David Duvenaud. 2020. Scalable Gradients for Stochastic Differential Equations. In *Proceedings of the Twenty Third International Conference on Artificial Intelligence and Statistics (Proceedings of Machine Learning Research, Vol. 108)*. Silvia Chiappa and Roberto Calandra (Eds.). PMLR, 3870–3882.
- [28] Richard Liaw, Eric Liang, Robert Nishihara, Philipp Moritz, Joseph E. Gonzalez, and Ion Stoica. 2018. Tune: A Research Platform for Distributed Model Selection and Training. <https://doi.org/10.48550/arXiv.1807.05118>
- [29] Bryan Lim, Sercan O. Arik, Nicolas Loeff, and Tomas Pfister. 2021. Temporal Fusion Transformers for interpretable multi-horizon time series forecasting. *International Journal of Forecasting* 37, 4 (Oct. 2021), 1748–1764. <https://doi.org/10.1016/j.ijforecast.2021.03.012>
- [30] Zachary C Lipton, David Kale, and Randall Wetzel. 2016. Directly Modeling Missing Data in Sequences with RNNs: Improved Classification of Clinical Time Series. In *Proceedings of the 1st Machine Learning for Healthcare Conference (Proceedings of Machine Learning Research, Vol. 56)*. Finale Doshi-Velez, Jim Fackler, David

Kale, Byron Wallace, and Jenna Wiens (Eds.). PMLR, Northeastern University, Boston, MA, USA, 253–270.

[31] Roderick J. A. Little and Donald B. Rubin. 2019. *Statistical Analysis with Missing Data*. John Wiley & Sons.

[32] Markus Löning, Anthony Bagnall, Sajaysurya Ganesh, Viktor Kazakov, Jason Lines, and Franz J. Király. 2019. sktime: A Unified Interface for Machine Learning with Time Series. <https://doi.org/10.48550/arXiv.1909.07872>

[33] Chris J. Maddison, Andriy Mnih, and Yee Whye Teh. 2017. The Concrete Distribution: A Continuous Relaxation of Discrete Random Variables. In *5th International Conference on Learning Representations, ICLR 2017, Toulon, France, April 24–26, 2017, Conference Track Proceedings*.

[34] Larry Medsker and Lakhmi C. Jain. 1999. *Recurrent Neural Networks: Design and Applications*. CRC Press.

[35] Philipp Moritz, Robert Nishihara, Stephanie Wang, Alexey Tumanov, Richard Liaw, Eric Liang, Melih Elbol, Zongheng Yang, William Paul, Michael I. Jordan, et al. 2018. Ray: A Distributed Framework for Emerging AI Applications. In *13th USENIX Symposium on Operating Systems Design and Implementation, OSDI 2018, Carlsbad, CA, USA, October 8–10, 2018*. 561–577.

[36] James Morrill, Christopher Salvi, Patrick Kidger, and James Foster. 2021. Neural Rough Differential Equations for Long Time Series. In *Proceedings of the 38th International Conference on Machine Learning, ICML 2021, 18–24 July 2021, Virtual Event*. 7829–7838.

[37] YongKyung Oh, Seungsu Kam, Jonghun Lee, Dong-Young Lim, Sungil Kim, and Alex Bui. 2025. Comprehensive Review of Neural Differential Equations for Time Series Analysis. <https://doi.org/10.48550/ARXIV.2502.09885>

[38] YongKyung Oh, Dongyoung Lim, and Sungil Kim. 2024. Stable Neural Stochastic Differential Equations in Analyzing Irregular Time Series Data. In *The Twelfth International Conference on Learning Representations, ICLR 2024, Vienna, Austria, May 7–11, 2024*. OpenReview.net.

[39] Yao Qin, Dongjin Song, Haifeng Chen, Wei Cheng, Guofei Jiang, and Garrison W. Cottrell. 2017. A Dual-Stage Attention-Based Recurrent Neural Network for Time Series Prediction. In *Proceedings of the Twenty-Sixth International Joint Conference on Artificial Intelligence, IJCAI 2017, Melbourne, Australia, August 19–25, 2017*. 2627–2633. <https://doi.org/10.24963/IJCAI.2017/366>

[40] Chotirat Ann Ratanamahatana and Eamonn Keogh. 2005. Three Myths about Dynamic Time Warping Data Mining. In *Proceedings of the 2005 SIAM International Conference on Data Mining (SDM)*. Society for Industrial and Applied Mathematics, 506–510. <https://doi.org/10.1137/1.9781611972757.50>

[41] Matthew A. Reyna, Christopher S. Josef, Russell Jeter, Supreeth P. Shashikumar, M. Brandon Westover, Shamim Nemati, Gari D. Clifford, and Ashish Sharma. 2020. Early Prediction of Sepsis From Clinical Data: The PhysioNet/Computing in Cardiology Challenge 2019. *Critical Care Medicine* 48, 2 (2020).

[42] Yulia Rubanova, Tian Qi Chen, and David Duvenaud. 2019. Latent Ordinary Differential Equations for Irregularly-Sampled Time Series. In *Advances in Neural Information Processing Systems 32: Annual Conference on Neural Information Processing Systems 2019, NeurIPS 2019, December 8–14, 2019, Vancouver, BC, Canada*. 5321–5331.

[43] Donald B. Rubin. 1976. Inference and missing data. *Biometrika* 63, 3 (1976), 581–592. <https://doi.org/10.1093/biomet/63.3.581>

[44] David E. Rumelhart, Geoffrey E. Hinton, and Ronald J. Williams. 1986. Learning representations by back-propagating errors. *Nature* 323, 6088 (Oct. 1986), 533–536. <https://doi.org/10.1038/323533a0>

[45] S. Hochreiter and J. Schmidhuber. 1997. Long Short-Term Memory. *Neural Computation* 9, 8 (Nov. 1997), 1735–1780. <https://doi.org/10.1162/neco.1997.9.8.1735>

[46] Shun-Yao Shih, Fan-Keng Sun, and Hung-yi Lee. 2019. Temporal pattern attention for multivariate time series forecasting. *Machine Learning* 108, 8 (Sept. 2019), 1421–1441. <https://doi.org/10.1007/s10994-019-05815-0>

[47] Satya Narayan Shukla and Benjamin M. Marlin. 2021. Multi-Time Attention Networks for Irregularly Sampled Time Series. In *9th International Conference on Learning Representations, ICLR 2021, Virtual Event, Austria, May 3–7, 2021*.

[48] Anh Tong, Thanh Nguyen-Tang, Dongeun Lee, Duc Nguyen, Toan M. Tran, David Leo Wright Hall, Cheongwoong Kang, and Jaesik Choi. 2025. Neural ODE Transformers: Analyzing Internal Dynamics and Adaptive Fine-tuning. In *The Thirteenth International Conference on Learning Representations, ICLR 2025, Singapore, April 24–28, 2025*.

[49] Belinda Tzen and Maxim Raginsky. 2019. Neural Stochastic Differential Equations: Deep Latent Gaussian Models in the Diffusion Limit. <https://doi.org/10.48550/arXiv.1905.09883>

[50] Ashish Vaswani, Noam Shazeer, Niki Parmar, Jakob Uszkoreit, Llion Jones, Aidan N Gomez, Łukasz Kaiser, and Illia Polosukhin. 2017. Attention is All you Need. In *Advances in Neural Information Processing Systems*, I. Guyon, U. Von Luxburg, S. Bengio, H. Wallach, R. Fergus, S. Vishwanathan, and R. Garnett (Eds.), Vol. 30. Curran Associates, Inc.

[51] Y. Lee, E. Jun, J. Choi, and H. -I. Suk. 2022. Multi-View Integrative Attention-Based Deep Representation Learning for Irregular Clinical Time-Series Data. *IEEE Journal of Biomedical and Health Informatics* 26, 8 (Aug. 2022), 4270–4280. <https://doi.org/10.1109/JBHI.2022.3172549>

[52] Jinsung Yoon, James Jordan, and Mihaela van der Schaar. 2018. GAIN: Missing Data Imputation using Generative Adversarial Nets. In *Proceedings of the 35th International Conference on Machine Learning, ICML 2018, Stockholm, Sweden, July 10–15, 2018*. 5675–5684.

[53] Jing Zhang, Peng Zhang, Baiwen Kong, Junqiu Wei, and Xin Jiang. 2021. Continuous Self-Attention Models with Neural ODE Networks. *Proceedings of the AAAI Conference on Artificial Intelligence* 35, 16 (May 2021), 14393–14401. <https://doi.org/10.1609/aaai.v35i16.17692>